Energy & Environmental Science

Accepted Manuscript

ROYAL SOCIETY OF CHEMISTRY

www.rsc.org/ees

Development of a hydrogen economy requires cheap and abundant electrocatalysts to achieve 4 key redox transformations: hydrogen evolution reaction (HER), hydrogen oxidation reaction (HOR), oxygen evolution reaction (OER) and oxygen reduction reactions (ORR). HER and OER take place in electrolyzers and photo-electrochemical cells (PECs) to produce hydrogen, and oxygen as a side product, from water while HOR and ORR are exploited in hydrogen fuels cells to produce electricity from hydrogen and oxygen (generally taken from the air). Platinum is so far the only material capable of catalyzing HER and HOR with performances suitable for proton-exchange membrane devices. We show here that a bio-inspired approach coupled with the proper structuration of the supporting materials allows to prepare molecular-engineered electrodes with high surface area and performances approaching those required for operational application in proton-exhange membrane fuels cells, electrolyzers and PECs.

Bio-inspired Noble Metal-Free Nanomaterials Approaching Platinum Performances for H_2 Evolution and Uptake

Tran N. Huan,[1,2,3] *Reuben T. Jane,*[1,2,3] *Anass Benayad,*[1, 4] *Laure Guetaz,*[1,4] *Phong. D. Tran*[1,2,3#] *and Vincent Artero*[1,2, 3]*

[1]Université Grenoble Alpes, Grenoble 38000 France

[2]Laboratory of Chemistry and Biology of Metals, CNRS UMR 5249, 17 rue des Martyrs, F-38054 Grenoble cedex 9 France

[3]Commissariat à l'énergie atomique et aux énergies alternatives (CEA), Life science Division, Grenoble 3800, France

[4]Commissariat à l'énergie atomique et aux énergies alternatives (CEA) ; Institut Laboratoire d'Innovation pour les Technologies des Energies Nouvelles et les Nanomatériaux (LITEN), Grenoble 3800, France

*To whom correspondence should be addressed. E-mail: vincent.artero@cea.fr

[#] Present address: University of Science and Technology of Hanoï, Hanoï, Vietnam.

Keywords: Hydrogenase Mimics, Nickel, Phosphine Ligands, Carbon Nanotubes, Pendant Proton Relays, Electrocatalysis; Surface Chemistry

Abstract

Hydrogen/water interconversion is a key reaction in the context of new energy technologies, including hydrogen fuel cells, water electrolyzers, and water-splitting photoelectrochemical cells. Specifications differ for these technologies to meet economic viability but state-of-the-art prototypes all rely on the powerful catalytic properties of platinum metal as catalyst for hydrogen production and uptake. Yet, this scarce and expensive metal is not itself a sustainable resource and its replacement by low cost and readily available materials is a requisite for these technologies to become economically viable. Here we revisit the preparation of bioinspired nanomaterials for hydrogen evolution and uptake (Le Goff et al. Science, 2009, 326, 1384-87) and show that molecular engineering combined with three

dimensional structuring of the electrode material allows the preparation of stable materials based on nickel bisdiphosphine catalytic units with performances in 0.5 M sulphuric acid aqueous electrolyte that approach those of commercial platinum-based materials (0.05 $mg_{Pt}.cm^{-2}$) assessed under similar, technologically relevant, operational conditions.

1. Introduction

Hydrogen production through the reduction of water appears to be one of the best long-term solutions for the storage of renewable energies. Water electrolysis with proton exchange membrane (PEM) devices is an attractive technology, owing to low internal resistance of the electrolytic cells, compactness, and possibility to operate bi-directionally, either storing energy in the form of hydrogen or releasing energy from hydrogen as supply/demand dictates (these devices are called Unitized Regenerative Fuel Cells). However, economically viable hydrogen production/uptake requires low and non-platinum catalysts since this expensive and scarce metal (only 37 ppb in the Earth's crust) is not a sustainable resource.[1] The US DOE road map for PEM fuel cell technology targets platinum group metal total loading of 0.125 $mg.cm^{-2}$ for both electrodes in 2020 [2] with state-of-the-art approaching 0.2 $mg_{Pt}.cm^{-2}$ for stable prototypes and a 3:1 distribution between cathode (0.15 $mg_{Pt}.cm^{-2}$) and anode (0.05 $mg_{Pt}.cm^{-2}$). Solutions exist to replace cathode oxygen reduction catalyst in H_2 PEM fuel cells (PEMFC) while meeting the above mentioned specifications [3-7] but no Pt-free hydrogen-oxidizing anode catalyst is available yet. The same is true for hydrogen evolution, as far as both power-biased water electrolysis (with cathode hydrogen-evolving catalysts specifications in PEM electrolysers similar as for anodes in PEM fuel cells) [8] or light-driven water splitting in photoelectrochemical (PEC) cells [9] are concerned. Most experimental demonstrations of solar-driven water splitting in PEC cells use Pt-based cathode catalysts able to sustain, at the lowest overpotential reported so far, the 20 $mA.cm^{-2}$ current density target corresponding to the solar photon flux.[10]

The last few years have seen the development of a number of high performing noble metal-free solid state inorganic catalysts capable of hydrogen evolution at low overpotentials,[11-13] yet not reaching thermodynamic equilibrium nor acting as bidirectional catalysts, a property still restricted to platinum metal, hydrogenases [14, 15] and some of their mimics.[16-19] The latter include the series of nickel bis(diphosphine) complexes

$[Ni(P^R_2N^{R'}_2)_2]^{2+}$ designed by D. L. DuBois and coworkers (Figure 1).[20] They combine a nickel center in an electron-rich environment, as found in the active site of [NiFe]-hydrogenases, with proton relays provided by a pendant base, mimicking the 2-aza-propane-1,3-dithiolato cofactor of [FeFe]-hydrogenases [21] and promoting the formation or activation of hydrogen (Figure 1). The combination of such a bioinspired molecular approach [20, 22, 23] with nanotechnological tools, through the attachment of $[Ni^{II}(P^R_2N^{R'}_2)_2]^{2+}$ mimics [14] on multi-wall carbon nanotubes (MWCNTs) allowed us to prepare a series of nickel-based nanomaterials with unique properties for bidirectional and reversible hydrogen evolution and uptake under conditions compatible with PEM technology.[17, 18] We recently implemented such materials in an operational noble metal-free PEMFC with a 0.74 V open circuit voltage.[24] We now report that such a bioinspired molecular engineering approach combined with three dimensional structuring allows the preparation of stable noble metal free nanomaterials with performances that approach and even outperform those of state-of-the-art platinum-based electrodes (0.05 $mg_{Pt}.cm^{-2}$) under technologically relevant operational conditions.

2. Experimental Section

Reagents and materials. Unless otherwise stated, chemicals including H_2SO_4 (98%), tetrabutylammonium tetrafluoroborate ($^nBu_4NBF_4$) (99%), dimethylformamide (DMF, 99.8%), acetonitrile (CH_3CN, 99.9%) and Nafion® solution (5% weight in a mixture of lower aliphatic alcohols) were purchased from Sigma-Aldrich. $[Ni(H_2O)_6](BF_4)_2$ was purchased from Acros Organics. UP-NC7000WT multi-walled carbon nanotubes (MWCNTs) were obtained from Nanocyl (purity >90% in carbon) and used as received. Carbon microfiber (7 µm diameter, 6 mm length) was purchased from Alfa Aesar. Pt/C (46 *wt.*% Pt / Vulcan XC72, Ref. TEC10V50) was purchased from Tanaka Kikinzoku Kogyo Co., Japan. The gas diffusion layer (GDL) substrate was purchased from GORE Fuel Cell Technologies (CARBEL CL-P-02360). (4-aminoethyl)benzene diazonium tetrafluoroborate was prepared according to literature procedures.[18, 25] $P^{Ph}_2N^{R_1}_2$ and $P^{Cy}_2N^{R_1}_2$ ligands (R_1 = *p*-$C_6H_4H_2CH_2CO_2$Pht, Pht = phthalimide as depicted in Figure 1) were synthesized as previously described (Ph and Cy designate phenyl and cyclohexyl substituents, respectively).[18] $[Ni(CH_3CN)_6](BF_4)_2$ was prepared as previously described.[26, 27]

Instrumentation. SEM images were recorded with a FEG-SEM (Leo 1530) operating at 5 kV. The X-ray photoelectron spectroscopy (XPS) analyses were performed with Φ PHYSICAL

ELECTRONICS versaProbe II spectrometer using a micro focused (diameter of the irradiated area = 200 μm) monochromatized Al Kα radiation (1486.6 eV). The residual pressure inside the analysis chamber was 7×10^{-8} Pa. The survey and the core level spectra were registered under a pass energy of 117.4 eV and 23.9 eV, respectively.

Electrochemical measurements. Electrochemical analysis was performed using a Bio-Logic science instrument SP300 potentiostat. Electrochemical experiments in CH_3CN (water content <50 ppm; tetrabutylammonium tetrafluoroborate $^nBu_4NBF_4$, 0.1 mol.L^{-1}, as the supporting electrolyte) were carried out in a three-electrode electrochemical cell under dry nitrogen atmosphere using the original modified electrodes described below as the working electrode, a platinum wire as the auxiliary electrode and a Ag/AgCl/KCl 3M reference electrode. The potential has been calibrated after each experiment by adding ferrocene in the solution and measuring its half-wave potential.

To reference potentials measured in CH_3CN to the standard hydrogen electrode (SHE), we used the experimentally determined value of $E^0(Fc/Fc^+)$ = 0. 43 V vs Ag/AgCl/KCl 3 mol.L^{-1} ($E_{Ag/AgCl}$ = 0.210 V vs SHE) and corrected it with the inter liquid potential (0.099 V)[28] between the aqueous electrolyte of the Ag/AgCl electrode and the CH_3CN solution containing $^nBu_4BF_4$ (0.1 mol.L^{-1}). This yields E_{CH_3CN} (Fc/Fc^+) = 0.53 V vs SHE. Such a value is close to that reported by Parker et al. [29] and coherent with the value reported by Addison and coworkers [30], once inter liquid potential (0.099 V) [28] between the aqueous electrolyte of the Ag/AgCl electrode and the CH_3CN solution is taken into account.

For electrocatalytic studies in CH_3CN, additions of protonated dimethylformamide ($DMFH^+$) introduced as an equimolar mixture of its triflate salt and DMF, [DMFH](OTf):DMF (1:1 mol/mol), were made with a syringe, using a freshly prepared 2:1 (mol:mol) mixture of dimethylformamide (4.9 mL) and triflic acid (2.8 mL) with a density of 1.28 and a $[DMFH]^+$ concentration of 4.1 M.

Characterization of functionalized MWCNT/GDL electrodes was achieved in 0.5 M H_2SO_4 (pH= 0.3) aqueous solution using the experimental set-up previously described.[18] A platinum wire acted as counter electrode and the reference was a mercury sulfate electrode (Radiometer MSE, Hg/Hg_2SO_4; E^0 = 0.68 V vs SHE). Polarization curves were conducted following the same test plan: while a pure hydrogen flow of 20 mL.min^{-1} was set, cyclic voltammetry (CV) from –1.00 V to –0.35 V vs $Hg/HgSO_4$ at 2 mV.s^{-1} were recorded. Hydrogen was generated from a H_2 generator (Innovative Gas System Company) with 99.8% purity of hydrogen.

For comparison, the commercial Pt/C (46% Pt) deposit on GDL was prepared using the same drop casting method (0.05 mg_{Pt} $.cm^{-2}$ GDL) and the cyclic voltammograms (CVs) were recorded for half-cell measurement at the same condition with Ni-based catalyst.

Preparation of MWCNT/GDL electrode.

Fabrication of classical MWCNT/GDL electrodes: MWCNTs (2 mg) were dispersed in 200 mL EtOH by sonication (1 h). Then, MWCNTs were deposited on 15 cm^2 GDL via filtration of the above solution onto the GDL placed over a Millipore Nylon membrane (HNWP 0.45 μm) and positioned on a Millipore Glass filtration Funnel operated under the water pump vacuum. Afterwards, the electrode was dried in the air before functionalization.

Fabrication of drop-cast MWCNT/GDL electrodes: MWCNTs (2 mg) were dispersed in 20 mL EtOH by sonication (1 h). Using the same system (for 15 cm^2 GDL), but without vacuum, and the nylon membrane was replaced by a paper towel extending over the filtration funnel. The paper towel thusly absorbed ethanol and transferred it by capillary action outside of the system where it evaporated, resulting in a slower deposition of MWCNT onto the GDL compared to the previous method. After 1 h, no solution remained on the top of the MWCNT/GDL and the electrode was dried in the air before functionalization.

Fabrication of MWCNT+carbon microfiber/GDL electrode: a mixture of MWCNT and carbon microfiber was dispersed in 20 mL EtOH by sonication (1 h). This suspension was deposited on GDL using the drop-casting system described above.

NiP^R_2-functionalized MWCNT/GDL electrode. Initially, the MWCNT/GDL was functionalized via the electro-reduction of (4-aminoethyl)benzene diazonium tetrafluoroborate to generate a poly-4-(2-aminoethyl)phenylene layer with free amine groups (as shown in Figure 1). Then the amino-functionalized MWCNT/GDL was grafted with the diphosphine ligand by immersion of the electrode overnight in 10 mL of a DMF solution containing 1 mM of the $P^{Ph}{}_2N^{R_1}{}_2$ ligand (or $P^{Cy}{}_2N^{R_1}{}_2$ ligand) and 2 mM of Et_3N (5.6 μL). Finally, the electrode was immersed in a 10 mL acetonitrile solution of 16 mg $[Ni(CH_3CN)_6](BF_4)_2$ or 10 mg $[Ni(H_2O)_6](BF_4)_2$ with overnight orbital stirring to yield the final functionalized MWCNT/GDL electrode. The functionalized MWCNT/GDL was then rinsed with acetonitrile and ethanol and dried in air. Finally, a thin Nafion film was deposited on the top of the electrode by dropping 100 μL of 5% Nafion solution on the electrode (15 cm^2). The membrane-electrode assembly was then air dried before use in further experiments.

3. Results and Discussion

In our previous work, nickel bis(diphosphine) functionalized MWCNT electrode materials were prepared by the grafting of pre-assembled $[Ni(P^{R}_2N^{R'}_2)_2](BF_4)_2$ complexes onto MWCNTs deposited on a gas-diffusion layer (GDL). Besides requiring a much higher amount of pre-synthesized complex than eventually attached onto the electrode surface, this method suffers from instability of the $[Ni(P^{R}_2N^{R'}_2)_2](BF_4)_2$ complexes under the conditions used to graft them covalently *via* amide-coupling. This reaction is carried out in the presence of the strong base triethylamine in dimethylformamide (DMF), conditions under which some $[Ni(P^{R}_2N^{R'}_2)_2](BF_4)_2$ *complexes* are not stable, but the *ligands* are. We therefore revisited our synthetic approach and investigated the possibility to construct the molecular catalytic sites in a stepwise manner on a MWCNT/GDL electrode, as presented in Figure 1. After deposition on the GDL, MWCNTs were first decorated with amine groups through diazonium grafting.[31] Then, ligands $P^{Ph}_2N^{R_1}_2$ or $P^{Cy}_2N^{R_1}_2$ (R_1 = *p*-$C_6H_4H_2CH_2CO_2$Pht with Pht = phthalimide as depicted in Figure 1, Ph and Cy represent phenyl and cyclohexyl substituents, respectively) were covalently immobilized on the surface of the electrode *via* amide coupling between these amino functions and the phthalimide activated ester moieties in the *para* position of the nitrogen-bound phenyl residues of the $P^{R}_2N^{R_1}_2$ ligands. The nickel centers were finally introduced with either the $[Ni(CH_3CN)_6](BF_4)_2$ complex as used before, or by $[Ni(H_2O)_6](BF_4)$, which work in our laboratory has shown to be equally good for formation of $[Ni(P^{R}_2N^{R'}_2)_2]^{2+}$ type complexes, and has the advantage of commercial availability, giving a further simplification of the synthetic process.[32]

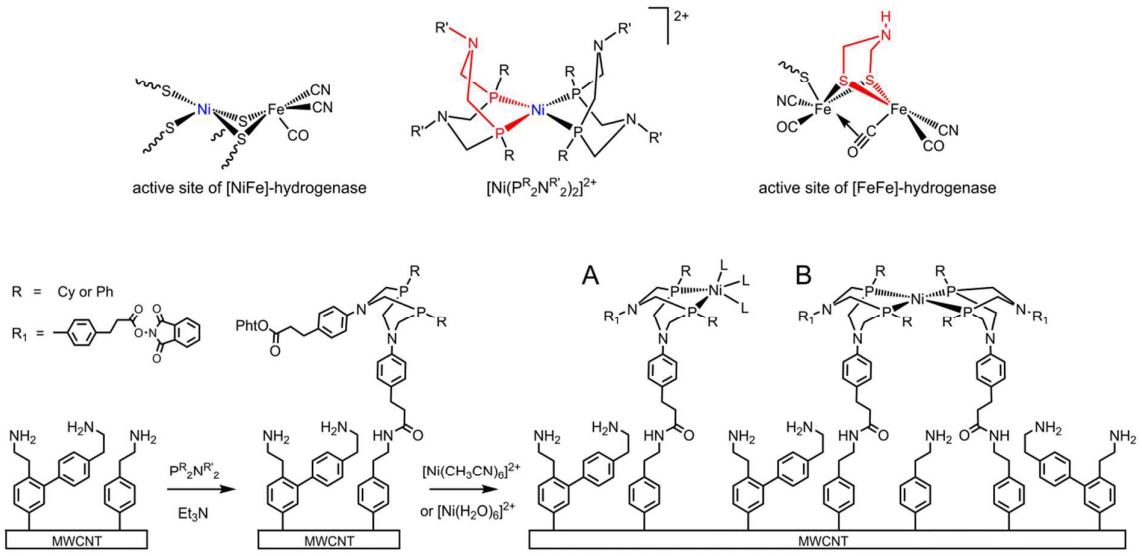

Figure 1. Top: A generic $[Ni(P^{R}_{2}N^{R'}_{2})_2]^{2+}$ complex, shown alongside the active sites of the [NiFe]- and [FeFe]-hydrogenases. Bottom: Procedure used to immobilize nickel diphosphine catalytic sites on MWCNT (L indicates solvent molecules).

X-ray photoelectron spectroscopy (XPS) analysis (Figure S1) confirms the presence of nickel(II)–phosphine complexes at the surface of the electrode. As found in previously reported materials,[17, 18] analysis of the Ni 2p3/2 region shows one sharp peak centered at 856.5 eV, which is a signature of the Ni^{II} ion, whereas the P 2p peak centered at 132.6 eV indicates the presence of metal-bound phosphorous atoms. Decomposition and quantification allowed a phosphorus/nickel ratio of 3 to be determined. Similar data have been obtained by Das et al. regarding surface immobilization of NiP^{R}_{2} moieties using Cu-catalyzed alkyne-azide cycloaddition chemistry.[33]We thus designate the grafted moieties as NiP^{R}_{2} (R = Cy or Ph) as at this stage we have no unambiguous evidence for their identity. It is possible that a single diphosphine ligand coordinates to each nickel center, with the coordination sphere completed by solvent molecules (Figure 1 A). Alternatively, two adjacent diphosphine ligands at the surface may form a $[Ni(P^{Cy}_{2}N^{R_1}_{2})_2]^{2+}$ complex, similar to the pre-synthesized catalyst used in our previous work (Figure 1 B). Of note, both these species may exist simultaneously.

The cyclic voltammograms (CV) of the NiP^{R}_{2}-functionalized (R = Cy or Ph) MWCNT/GDL electrodes in acetonitrile with 0.1M $^{n}Bu_4NBF_4$ as supporting electrolyte display two quasi-reversible cathodic processes at –1.28 V and –1.03 V versus Fc/Fc^{+}, and at –1.26 V and –1.02 V versus Fc/Fc^{+} for the NiP^{Cy}_{2} and NiP^{Ph}_{2}-functionalized electrodes, respectively (Figure S2). These are likely to be a combination of the two one-electron waves observed for Ni(II/I) and Ni(I/0) as previously reported.[20] The integration of these waves allows surface concentrations of 2.85 (± 0.5) × 10^{-9} mol.cm^{-2} and 3.05 (± 0.5) × 10^{-9} mol.cm^{-}

^{2} to be determined for the NiP^{Cy}_2 and NiP^{Ph}_2-functionalized electrodes, respectively. Such values are approximately twice as high as the catalyst surface concentration previously reported.[18] Accordingly, the proton reduction activities of the NiP^{R}_2-functionalized electrode materials, investigated in the presence of protonated dimethylformamide in CH_3CN (Figure S3), were significantly higher than that of the grafted pre-synthesized catalyst in our previous work.[20]

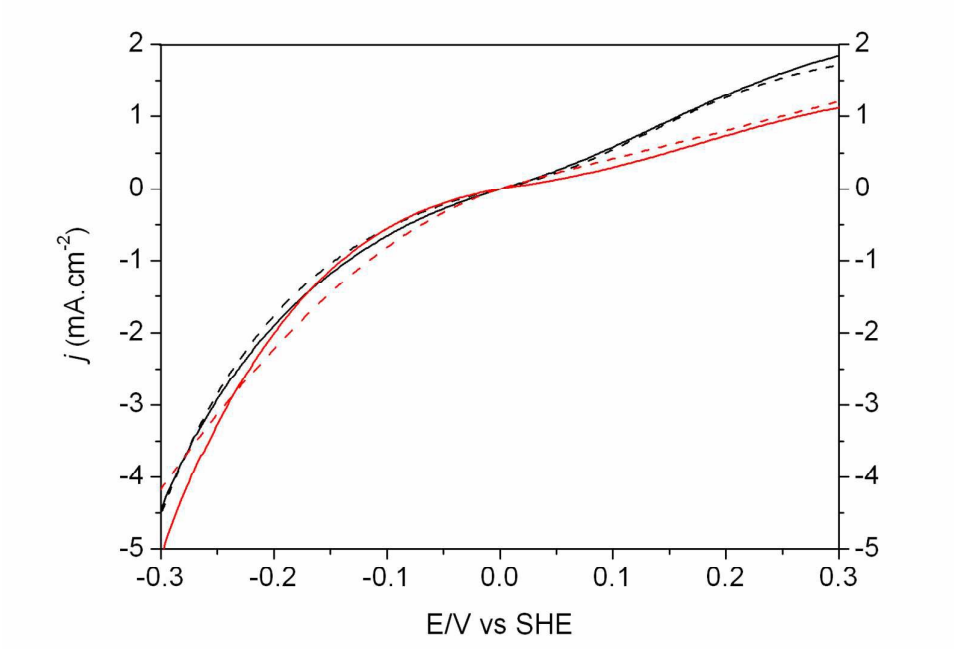

Figure 2. Comparison of the catalytic activity of NiP^{Cy}_2 (black) and NiP^{Ph}_2 (red) complexes synthesized from $[Ni(CH_3CN)_6](BF_4)_2$ (solid traces) and $[Ni(H_2O)_6](BF_4)_2$ (dashed traces) on a 0.133 mg MWCNT/cm^2 GDL electrode. Data are not compensated for ohmic drop.

Detailed investigation of the catalytic activity of the novel materials has been carried out in 0.5 M H_2SO_4 aqueous solution using a previously described half-cell configuration which reproduces the experimental conditions found in proton-exchange membrane electrolysers.[18] A membrane-electrode assembly (MEA) has been prepared for this purpose by drop-casting a hydro-alcoholic Nafion solution on the top of the NiP^{R}_2-functionalized MWCNT/GDL electrode. In order to ensure a fair comparison between the two different diphosphine ligands without other possible variation, an amino-functionalized MWCNT/GDL electrode was cut into two smaller electrodes and each half was functionalized as stated above with either the $P^{Cy}_2N^{R_1}_2$ or $P^{Ph}_2N^{R_1}_2$ ligand (R_1 = *p*-$C_6H_4H_2CH_2CO_2Pht$). These electrodes were then reacted with $[Ni(CH_3CN)_6](BF_4)_2$, and the activities of the resulting NiP^{Ph}_2 and NiP^{Cy}_2 catalysts in the half-cell experiment are presented in Figure 2. The linear voltammetry recorded from –300 mV to +300 mV vs the standard hydrogen electrode (SHE) demonstrates

reversible catalytic activity with transition between hydrogen production and oxidation occurring at the point of 0 V vs SHE, which corresponds to the thermodynamic potential of the H^+/H_2 couple when $a(H^+) = 1$, $P_{H2} = 10^5$ Pa, and at 25 °C. The current density obtained for hydrogen production at –300 mV vs SHE is a little bit higher for NiP^{Ph}_2 than for NiP^{Cy}_2, while for hydrogen oxidation at +300 mV vs SHE, the current density of 2 $mA.cm^{-2}$ obtained with NiP^{Cy}_2 is significantly higher than the 1 $mA.cm^{-2}$ of NiP^{Ph}_2. This result is in agreement with previous reports, which suggest catalysts with phenyl groups at the phosphorous are more suited to hydrogen production, whereas those with cyclohexyl groups are more suited to hydrogen oxidation.[17, 34] The same experiments have been carried out under nitrogen atmosphere to confirm that no oxidation current was observed in the absence of hydrogen (Figure S4). Similarly, nickel-free electrodes do not display any significant catalytic activity (Figure S4). Figure 2 also displays the polarization curves obtained for the electrode materials prepared using $[Ni(H_2O)_6](BF_4)_2$ as the source of nickel cations. Remarkably, these electrodes show comparable activity in the half-cell experiment to those prepared using the $[Ni(CH_3CN)_6](BF_4)_2$ precursor. This novel on-surface stepwise construction of nickel diphosphine catalytic sites thus proves to be much more straightforward than the previously described procedure, short-cutting the synthesis of both $[Ni(CH_3CN)_6](BF_4)_2$ and $[Ni(P^R_2N^{R'}_2)_2](BF_4)_2$ complexes, without bringing any detrimental effect to the catalytic performances of the final electrodes.

In the following, we show that such performances can be further significantly improved through optimization of the three dimensional structure of the electrode material. Initial attempts to increase current density for H_2 oxidation *via* the fabrication of thicker MWCNT/GDL electrodes failed, which indicated a possible limitation due to H_2 diffusion within the electrode.[17, 24] A less compact MWCNT/GDL electrode should be a better substrate, its greater surface area allowing the grafting of more catalyst molecules, and its porosity facilitating diffusion of hydrogen. To verify this hypothesis, we prepared less compact electrodes using a drop-casting method to deposit the MWCNT mat onto the GDL. By comparison with the previously used filtration method, the new electrodes are 20% thicker for the same amount of MWCNTs, as revealed by cross section scanning electron microscopy (SEM) images (Figure S5). These electrodes accordingly showed a significant increase of activity for both hydrogen production and oxidation as compared to electrodes constructed using the vacuum filtration method. As shown in Figure S6 (black and red traces), the current densities measured at 300 mV overpotential for hydrogen production and oxidation increase from 5.9 to 10.5 $mA.cm^{-2}$ and 1.98 to 3.4 $mA.cm^{-2}$, respectively. The increase of current

density is directly related to the increased amount of grafted NiP^{Cy}_2 catalyst on MWCNTs drop casting electrode, which has been calculated to be 5.0 (± 0.5) × 10^{-9} mol.cm^{-2} by cyclic voltammetry of the modified electrode in acetonitrile. This confirmed our hypothesis that the catalytic performance of the material can be improved by changing the method of constructing the MWCNT/GDL electrode to obtain a highly porous substrate.

An extension of these findings was explored, in which the use of carbon micro-fibers mixed with the MWCNT before deposition onto the GDL electrode was investigated to produce an electrode with ultra-high surface area and more permeable to hydrogen gas. With an average diameter of 7 μm and an average length of 6 mm, the microfibers are very large compared to the MWCNTs, and it was expected that MWCNTs would adsorb on the surface of the microfibers, and the relatively large space between fibers would facilitate the diffusion of both the electrolyte and hydrogen gas. An initial test using the same amount of MWCNTs as used previously, along with 50% w/w carbon microfiber showed an improvement in the catalytic activity of the material (Figure S6, blue trace). After optimization of the relative quantities of MWCNTs and microfibers, the best performances were obtained with an electrode comprising 0.267 mg MWCNTs and 0.033 mg carbon microfiber per square centimeter of GDL (Figure S6, green trace). Characterization of the electrode was performed by SEM (Figure 3). The crossing of the microfibers to form a porous network can be seen in both the top down (A) and side on (B) views. Comparison of the cross section, with thickness of 18-20 μm, to that of the simple drop cast electrode without carbon microfibers (4 μm, Figure S5) shows the large increase in the porosity of the layers. Magnified views C and D confirm that the microfibers are coated with a thin layer of carbon nanotubes.

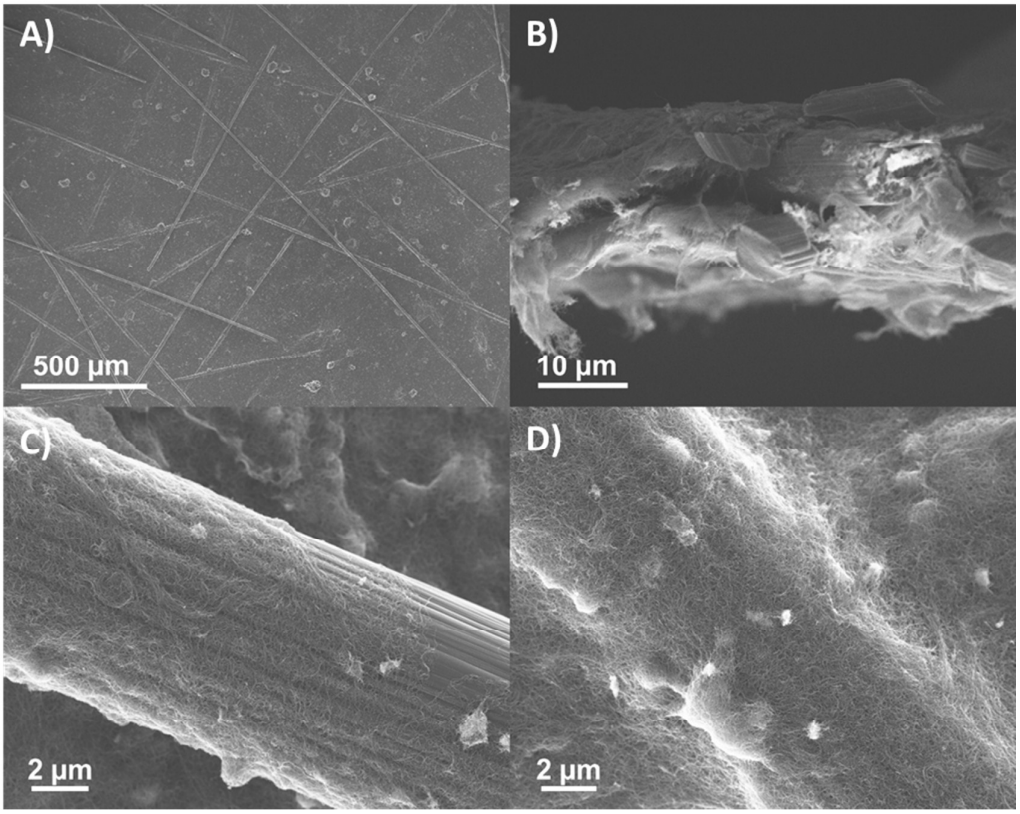

Figure 3. SEM images of GDL electrode coated with 0.267 mg cm^{-2} MWCNT and 0.033 mg cm^{-2} carbon microfiber. A) top view; B) cross-section view; C) and D) magnification showing single carbon microfibers coated with MWCNTs.

The effect of the increased surface area of the porous structure is also reflected in the amount of NiP^{Cy}_2 catalyst grafted on the electrode, which has been shown by cyclic voltammetry to be 2.5×10^{-8} mol.cm^{-2}, a fivefold increase compared with the drop-cast MWCNT/GDL electrode. This MWCNT+carbon microfiber/GDL electrode showed catalytic performance of 16 mA.cm^{-2} at –300 mV vs SHE for hydrogen production and 13.2 mA.cm^{-2} at +300 mV vs SHE for hydrogen oxidation at room temperature (black trace in Figure 4). It outperforms, in current density for hydrogen oxidation at +300 mV vs SHE and amount of grafted nickel catalyst, electrodes made with the same amount of MWCNT but with either reduced amounts (0.0166 mg) of carbon microfiber (6.8 mA cm^{-2}, 1.1×10^{-8} mol.cm^{-2}), or no carbon microfiber at all (3.96 mA cm^{-2}, 6.1×10^{-9} mol.cm^{-2}, Figure S7). Blank experiments under nitrogen or using an unfunctionalized electrode show no current for hydrogen oxidation, even at 85°C (Figure S8). The ratio between current densities at 100 mV overpotential for hydrogen oxidation and production ($j_{oxidation}/j_{production}$) is found to be 0.86 for the MWCNT+carbon microfiber electrode, which is significantly higher than the value of

~0.5 obtained for all electrodes based on MWCNT alone as the substrate. This suggests improved diffusion of the hydrogen gas through the porous structure to the catalyst active site.

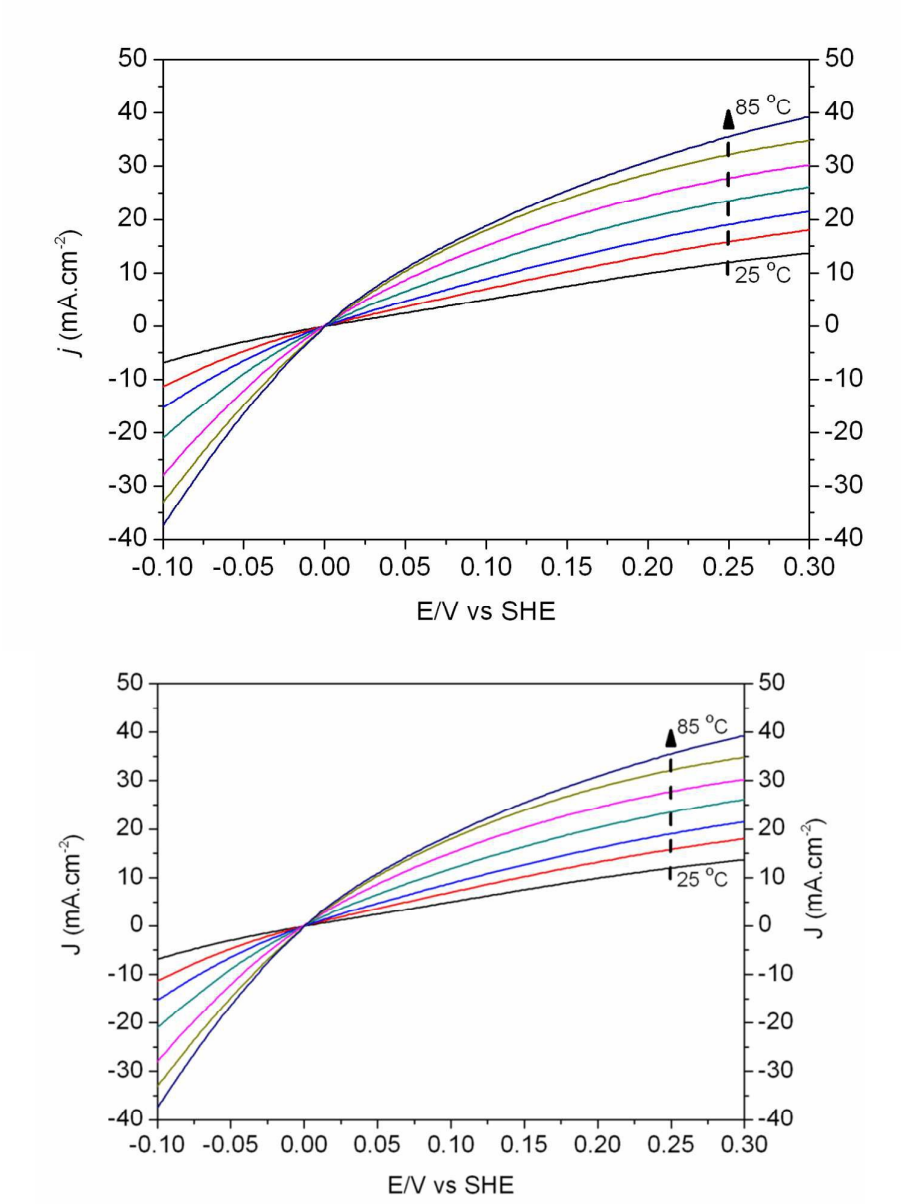

Figure 4. Catalytic activity of NiP^{Cy}_2 grafted on a 0.267 mg cm^{-2} MWCNT and 0.033 mg cm^{-2}carbon micro-fiber GDL in the half-cell experiment at various temperatures. Potentials were referred to SHE, the potential of which was calculated at each temperature using the Nernst equation. Data are not compensated for ohmic drop.

The catalytic performance of the electrode at elevated temperatures was also investigated, as this corresponds to typical operational conditions in fuel cells or electrolyzers. The temperature was varied from 25°C to 85°C and the polarizations of the electrode were recorded at intervals of 10°C. Again, reversible activity was observed, with open circuit potential exactly corresponding to the thermodynamic equilibrium of the H^+/H_2 couple at each

temperature. As shown in Figure 3, the current obtained for hydrogen oxidation dramatically increased at elevated temperatures. At 85°C, a current of 40 mA.cm^{-2} was observed at +300 mV vs SHE, a 2.85 times enhancement of the current obtained at 25°C, corresponding to an activation energy of 14.5 ± 0.3 kJ.mol^{-1}. Hydrogen production showed an even greater enhancement at elevated temperature, with a fivefold increase of current observed at 85°C compared to that at 25°C, corresponding to an activation energy of 23 ± 1 kJ.mol^{-1}. Similar results have been obtained with NiP^{Ph}_2-functionalized electrodes (Figure S9). Such low and distinct activation energy values for hydrogen production and oxidation are comparable to those measured for Pt-based MEAs[35] and indicate that the current is not limited by the intrinsic turnover frequency of the grafted catalyst, but rather by mass transport of protons and hydrogen gas in the bulk of the electrode material.[24]

The long term stability of the MWCNT+carbon microfiber electrode for hydrogen oxidation and production was tested at +300 mV and –100 mV vs SHE, respectively. It proved to be stable for both hydrogen oxidation and production over 7 hours of electrolysis at room temperature, corresponding to 21000 turnovers for hydrogen oxidation (Figure S10A). However, the current density for hydrogen oxidation was less stable over time when measured at either 55°C or 85°C (Figure S10B and S11B): After 40 minutes at 55°C, the current had decreased from 35.0 mA.cm^{-2} to 16.0 mA.cm^{-2}, and after 40 minutes at 85°C the current had decreased from 39.4 mA.cm^{-2} to 20.4 mA.cm^{-2}. This loss of current is not observed when the reverse reaction, i.e. hydrogen production is achieved at –100 mV vs SHE at 55°C (Figure S11B). A polarization curve recorded after 1h electrolysis at +300 mV vs SHE clearly reflects the decrease in hydrogen oxidation activity compared to the initial electrode, while showing unmodified hydrogen evolution activity (Figure S11A). We thus exclude decomposition of the catalytic sites as the reason for such an evolution of the performance during operation. Such a decrease of the hydrogen oxidation current upon use is therefore likely caused by material structure collapse or bad water management within the membrane electrode assembly. We note that a similar decrease of current densities during continuous operation at high temperature is observed for Pt-based MEAs (Figure S12).

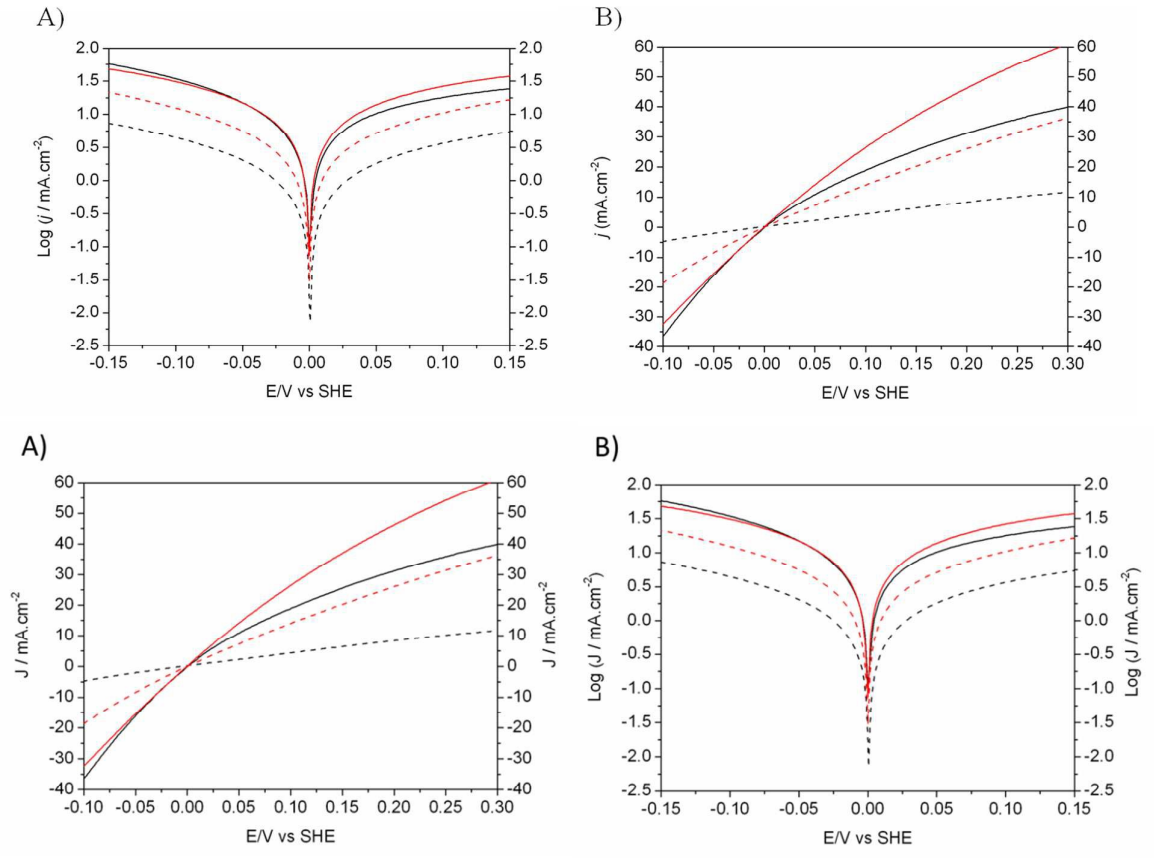

Figure 5. Catalytic activity for hydrogen evolution and oxidation (A) and Tafel plots obtained from linear sweep voltammetry experiments recorded at 2 $mV.s^{-1}$ (B) of the NiP^{Cy}_2-functionalized MWCNT+carbon microfiber electrode (black) and the Pt/C electrode (0.05 $mg_{Pt}.cm^{-2}$) (red) at 25°C (dashed trace) and 85°C (solid trace) in 0.5 M H_2SO_4. Data are not compensated for ohmic drop.

In Figure 5 we compare the activity of the NiP^{Cy}_2-functionalized MWCNT+carbon microfiber electrode to that of a MEA prepared using the same procedure but with commercially available highly dispersed platinum nanoparticles deposited onto carbon black (Pt/C 46% weight) as catalyst. The same Pt/C material has been used in other studies.[35-37] We selected a Pt loading (0.05 $mg_{Pt}.cm^{-2}$) corresponding to that typically used for the H^+/H_2 interconverting electrode in unitized regenerative fuel cells. The total amount of platinum present in the electrode (2.5×10^{-7} $mol.cm^{-2}$) is ten-fold higher than the 2.5×10^{-8} $mol.cm^{-2}$ surface concentration of the nickel complex. At 25°C, the NiP^{Cy}_2-functionalized MWCNT+carbon microfiber containing MEA shows current densities less than one order of magnitude lower than those of the Pt-containing MEA (dashed traces in Figure 5). However at 85°C, polarization curves measured at Ni and Pt-based electrodes become comparable. Table 1 summarizes the performances of both Ni and Pt-based electrodes materials for hydrogen evolution at 100 mV overpotential and hydrogen oxidation at 100 mV and 300 mV

overpotential. The Ni-based electrode is only ~35% less active for hydrogen oxidation at 85°C, and outperforms the platinum catalyst for hydrogen production at the same temperature by ~20%. Measurements performed in this study are obtained under half-cell configuration, with significantly higher resistance between the working AME and the counter-electrode than in full cell configurations. Therefore comparison with other studies may not be straightforward. We also note that the performances of Pt-based electrodes vary over several orders of magnitude depending on the MEA preparation procedure.[36] The classical procedures used to assemble the Nafion membrane with catalytic layers so as to optimize the interface and reduce mass-transport limitations require high pressure and high temperatures that are not withstand by our Ni-based electrode materials. We therefore had to adapt the experimental protocol for the MEA preparation as described above. As a consequence the performances of the Pt-based electrodes used here for comparison lie in the lower range of previously reported values.[36] Much better current densities can also be measured for Pt-based MEA u sing specific hydrogen-pump setup.[35, 36]

Regarding hydrogen evolution[38] in PEC cells, the relevant figures of merit is the overpotential required to reach current density of 10 or 20 $mA.cm^{-2}$.[39] Earth-abundant materials, such as NiMo and NiMoCo alloys compare well with Pt in that prospect with overpotential requirement of 45-55 mV to reach 10 $mA.cm^{-2}$ at room temperature.[39] A higher overpotential value is required to reach this current density value at room temperature for the NiP^{Cy}_2-functionalized MWCNT+carbon microfiber electrode. However, higher temperature are more relevant under operating conditions for PEC devices. As shown in Figure S13, the NiP^{Cy}_2-functionalized MWCNT+carbon microfiber electrode requires only 32 and 60 mV to reach 10 or 20 $mA.cm^{-2}$ current density values at 85°C, which is nearly identical to that of the platinum MEA (32 and 61 mV, respectively).

Table 1. Current obtained for hydrogen oxidation at 100 mV and 300 mV overpotential, and for hydrogen evolution at 100 mV overpotential with the NiP^{Cy}_2-functionalized MWCNT+carbon microfiber (2.5×10^{-8} $mol_{Ni}.cm^{-2}$) and Pt/C (2.5×10^{-7} $mol_{Pt}.cm^{-2}$) electrodes at 25°C and 85°C.

	E vs SHE	NiP^{Cy}_2 (2.5×10^{-8} $mol_{Ni}.cm^{-2}$)	Pt/C (2.5×10^{-7} $mol_{Pt}.cm^{-2}$)
25°C	+100 mV (H_2 ox)	6.1 mA cm^{-2}	14.0 mA cm^{-2}
	+300 mV (H_2 ox)	11.67 mA cm^{-2}	36.4 mA cm^{-2}
	–100 mV (H_2 prod)	7.1 mA cm^{-2}	18.4 mA cm^{-2}
85°C	+100 mV (H_2 ox)	16.8 mA cm^{-2}	26.6 mA cm^{-2}
	+300 mV (H_2 ox)	40.1 mA cm^{-2}	60.9 mA cm^{-2}
	–100 mV (H_2 prod)	38.3 mA cm^{-2}	32.2mA cm^{-2}

4. Conclusion

This study shows that cost-effective, molecular-engineered bio-inspired nanomaterials are likely to approach and even exceed the performance of platinum-based electrodes under technologically relevant conditions. Such performances rely on efficient functionalization of MWCNTs coupled with controlled three dimensional structuring of the electrode support. The high surface area and electrical conductivity of MWCNTs are key aspects in this context to avoid passivation of the electrode surface upon functionalization.[31] Future studies will target other nano-architectures with controlled porosity, which may provide long term stability for hydrogen oxidation at high temperatures, optimization of the bio-inspired catalyst-membrane interface in MEA and implementation into operational PEM devices. This methodology may also be extended to other bioinspired molecular systems targeting key energy-related multielectronic reactions such as O_2 reduction, water oxidation, CO_2 reduction or N_2 fixation.

Electronic Supplementary Information. XPS spectra of NiP^{Cy}_2-functionalized MWCNT/GDL electrode, additional SEM images, cyclic and linear voltammograms and control experiments.

Authors Contributions

TNH, RTJ and PDT performed experiments; AB and LG contributed to XPS and SEM characterization; VA designed research and wrote the paper. All authors have given approval to the final version of the manuscript.

Acknowledgements

This work was supported by ANR (Caroucell project, ANR-13-BIME-003 and Labex program ARCANE, ANR-11-LABX-0003-01) and the FCH Joint Undertaking (Nano-Cat project, grant n° 325239). The authors thank Nicolas Guillet (CEA/LITEN) for helpful discussion and help during the analysis of the data.

References

1. A. Brouzgou, S. Q. Song and P. Tsiakaras, *Applied Catalysis B: Environmental*, 2012, **127**, 371-388.

2. F. C. t. O. U.S. Department of Energy, 2012.
3. M. E. Scofield, H. Liu and S. S. Wong, *Chem. Soc. Rev.*, 2015, **44**, 5836-5860.
4. R. Bashyam and P. Zelenay, *Nature*, 2006, **443**, 63-66.
5. M. Lefevre, E. Proietti, F. Jaouen and J. P. Dodelet, *Science*, 2009, **324**, 71-74.
6. K. P. Gong, F. Du, Z. H. Xia, M. Durstock and L. M. Dai, *Science*, 2009, **323**, 760-764.
7. A. Morozan, B. Jousselme and S. Palacin, *Energy Environ. Sci.*, 2011, **4**, 1238-1254.
8. N. Armaroli and V. Balzani, *ChemSusChem*, 2011, **4**, 21-36.
9. M. G. Walter, E. L. Warren, J. R. McKone, S. W. Boettcher, Q. Mi, E. A. Santori and N. S. Lewis, *Chem. Rev.*, 2010, **110**, 6446-6473.
10. J. W. Ager III, M. Shaner, K. Walczak, I. D. Sharp and S. Ardo, *Energy Environ. Sci.*, 2015, DOI: 10.1039/C1035EE00457H.
11. J. R. McKone, E. L. Warren, M. J. Bierman, S. W. Boettcher, B. S. Brunschwig, N. S. Lewis and H. B. Gray, *Energy Environ. Sci.*, 2011, **4**, 3573-3583.
12. E. J. Popczun, J. R. McKone, C. G. Read, A. J. Biacchi, A. M. Wiltrout, N. S. Lewis and R. E. Schaak, *J. Am. Chem. Soc.*, 2013, **135**, 9267-9270.
13. A. B. Laursen, K. R. Patraju, M. J. Whitaker, M. Retuerto, T. Sarkar, N. Yao, K. V. Ramanujachary, M. Greenblatt and G. C. Dismukes, *Energy Environ. Sci.*, 2015, **8**, 1027-1034.
14. W. Lubitz, H. Ogata, O. Rüdiger and E. Reijerse, *Chem. Rev.*, 2014, **114**, 4081-4148.
15. F. A. Armstrong, N. A. Belsey, J. A. Cracknell, G. Goldet, A. Parkin, E. Reisner, K. A. Vincent and A. F. Wait, *Chem. Soc. Rev.*, 2009, **38**, 36-51.
16. T. R. Simmons, G. Berggren, M. Bacchi, M. Fontecave and V. Artero, *Coord. Chem. Rev.*, 2014, **270–271**, 127-150.
17. P. D. Tran, A. Le Goff, J. Heidkamp, B. Jousselme, N. Guillet, S. Palacin, H. Dau, M. Fontecave and V. Artero, *Angew. Chem. Int. Ed.*, 2011, **50**, 1371-1374.
18. A. Le Goff, V. Artero, B. Jousselme, P. D. Tran, N. Guillet, R. Metaye, A. Fihri, S. Palacin and M. Fontecave, *Science*, 2009, **326**, 1384-1387.
19. S. E. Smith, J. Y. Yang, D. L. DuBois and R. M. Bullock, *Angew. Chem. Int. Ed.*, 2012, **51**, 3152-3155.
20. D. L. DuBois, *Inorg. Chem.*, 2014, **53**, 3935-3960.
21. G. Berggren, A. Adamska, C. Lambertz, T. R. Simmons, J. Esselborn, M. Atta, S. Gambarelli, J. M. Mouesca, E. Reijerse, W. Lubitz, T. Happe, V. Artero and M. Fontecave, *Nature*, 2013, **499**, 66-69.
22. M. Fontecave and V. Artero, *C. R. Chim.*, 2011, **14**, 362-371.
23. A. D. Wilson, R. H. Newell, M. J. McNevin, J. T. Muckerman, M. R. DuBois and D. L. DuBois, *J. Am. Chem. Soc.*, 2006, **128**, 358-366.
24. P. D. Tran, A. Morozan, S. Archambault, J. Heidkamp, P. Chenevier, H. Dau, M. Fontecave, A. Martinent, B. Jousselme and V. Artero, *Chem. Sci.*, 2015, **6**, 2050-2053.
25. S. Griveau, D. Mercier, C. Vautrin-Ul and A. Chaussé, *Electrochem. Commun.*, 2007, **9**, 2768-2773.
26. B. J. Hathaway and A. E. Underhill, *J. Chem. Soc.*, 1960, 3705-3711.
27. B. J. Hathaway, D. G. Holah and A. E. Underhill, *J. Chem. Soc.*, 1962, 2444-2448.
28. C. Costentin, S. Drouet, M. Robert and J. M. Saveant, *Science*, 2012, **338**, 90-94.
29. V. D. Parker, K. L. Handoo, F. Roness and M. Tilset, *J. Am. Chem. Soc.*, 1991, **113**, 7493-7498.
30. V. V. Pavlishchuk and A. W. Addison, *Inorg. Chim. Acta*, 2000, **298**, 97-102.
31. A. Le Goff, F. Moggia, N. Debou, P. Jegou, V. Artero, M. Fontecave, B. Jousselme and S. Palacin, *J. Electroanal. Chem.*, 2010, **641**, 57-63.
32. R. T. Jane, P. D. Tran, E. S. Andreiadis, J. Pécaut and V. Artero, *C. R. Chimie*, 2015, **18** 752-757.
33. A. K. Das, M. H. Engelhard, S. Lense, J. A. S. Roberts and R. M. Bullock, *Dalton Trans.*, 2015, **44**, 12225-12233.
34. W. J. Shaw, M. L. Helm and D. L. DuBois, *Biochim. Biophys. Acta Bioenerg.*, 2013, **1827**, 1123-1139.
35. J. Durst, C. Simon, F. Hasché and H. A. Gasteiger, *J. Electrochem. Soc.*, 2015, **162**, F190-F203.

36. K. C. Neyerlin, W. Gu, J. Jorne and H. A. Gasteiger, *J. Electrochem. Soc.*, 2007, **154**, B631-B635.
37. W. Sheng, H. A. Gasteiger and Y. Shao-Horn, *J. Electrochem. Soc.*, 2010, **157**, B1529-B1536.
38. N. Danilovic, R. Subbaraman, D. Strmcnik, V. R. Stamenkovic and N. M. Markovic, *J. Serb. Chem. Soc.*, 2013, **78**, 2007-2015.
39. C. C. L. McCrory, S. Jung, I. M. Ferrer, S. M. Chatman, J. C. Peters and T. F. Jaramillo, *J. Am. Chem. Soc.*, 2015, **137**, 4347-4357.